MELINDA: A Multimodal Dataset for Biomedical Experiment Method Classification

Te-Lin Wu[1], **Shikhar Singh**[2], **Sayan Paul**[3], **Gully Burns**[4], **Nanyun Peng**[1]

[1] University of California, Los Angeles, [2] University of Southern California
[3] Intuit Inc., [4] Chan Zuckerberg Initiative
{telinwu, violetpeng}@cs.ucla.edu[1], ssingh43@usc.edu[2], sayan.paul6@gmail.com[3], gully.burns@chanzuckerberg.com[4]

Abstract

We introduce a new dataset, MELINDA, for **M**ultimodal biom**E**dica**L** exper**I**me**N**t metho**D** cl**A**ssification. The dataset is collected in a fully automated *distant supervision* manner, where the labels are obtained from an existing curated database, and the actual contents are extracted from papers associated with each of the records in the database. We benchmark various state-of-the-art NLP and computer vision models, including unimodal models which only take either caption texts or images as inputs, and multimodal models. Extensive experiments and analysis show that multimodal models, despite outperforming unimodal ones, still need improvements especially on a less-supervised way of grounding visual concepts with languages, and better transferability to low resource domains. We release our dataset and the benchmarks to facilitate future research in multimodal learning, especially to motivate targeted improvements for applications in scientific domains.

Introduction

Biocuration, the activity of *manually* organizing biological information, is a crucial yet human-effort-intensive process in biomedical research (ISB 2018). Organizing such knowledge in a structured way is important for accelerating science since it facilitates downstream tasks such as scientific information retrieval (Craven, Kumlien et al. 1999; Mohan et al. 2018; Burns et al. 2018; Burns, Li, and Peng 2019), and question answering (Ben Abacha et al. 2019; Nguyen et al. 2019; He et al. 2020).

One such curation task is recognizing *experiment methods*, which identifies the underlying experimental protocols that result in the figures in research articles. It can be formulated as a multi-class classification task, which takes as inputs the figures and their captions, and outputs the corresponding experiment types that generate the figures, as illustrated in Figure 1.

The task is inherently *multimodal* as biocurators need to take both the figure and the caption into consideration to make their decisions (Demner-Fushman et al. 2012).[1] While scientists can do the task with perfect accuracy, the requirements of manual labeling from experts hinder the scalability of the process. It is thus imperative to develop advanced language and computer vision multimodal tools to help accelerate the aforementioned scientific discovery process.

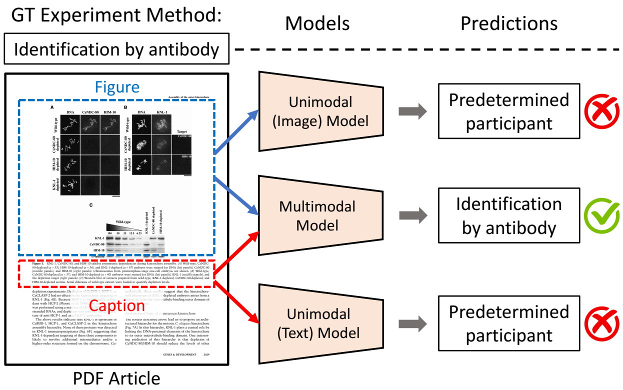

Figure 1: The MELINDA dataset & the biomedical experiment classification task: We introduce a new dataset which concerns learning to recognize the underlying experiment methods used to produce an experimental figure in biomedical research articles. The recognition is fundamentally multimodal, where justification of the experiment methods takes both figures and captions into consideration. The MELINDA dataset could serve as a good testbed for benchmarking, as well as motivating multimodal models particularly in biomedical and low-resource domains.

However, automatically identifying the experiment methods poses significant challenges for multimodal processing tools. One major challenge is how to ground the visual concepts to language. Most current visual-linguistics multimodal models (Li et al. 2019; Lu et al. 2019; Su et al. 2020; Chen et al. 2020) rely on a robust *object detection* module to identify *predefined* objects for grounding finer granularity of visual and linguistics concepts. However, as it requires extra efforts from experts, scientific images often lack ground truth object annotations, and the transfer of pretrained detection models suffers from significant domain shifts. As a result, this specific domain would appreciate multimodal mod-

[1] Although different experiment methods tend to generate visually different results, the differences can be subtle and the captions often help distinguish these subtle differences among figures.

els particularly with less-supervised grounding paradigms. In addition, it is expensive to collect annotations from domain experts; the lack of sizable benchmark datasets hinders the development of multimodal models tailored to the biomedical domain.

To spur research in this area, we introduce MELINDA, a dataset for **M**ultimodal biom**E**dica**L** exper**I**me**N**t metho**D** cl**A**ssification that is created through a fully automated *distantly supervised* process (Mintz et al. 2009). Specifically, we leverage an existing biomedical database, **IntAct**[2] (Orchard et al. 2013), to get the experiment method labels, and then properly extract the actual contents from papers pointed by the records in IntAct to pair with the obtained labels. MELINDA features 2,833 figures paired with their corresponding captions.We further segment captions into subcaptions referring to different sub-figures in the images, resulting in a total of 5,371 data records along with the labels of the experiment methods used to generate the sub-figures.

We benchmark several state-of-the-art models on the proposed experiment method classification task, including unimodal vision and language models and multimodal ones. Experiments suggest that multimodality is helpful for achieving better performances. However, the performances are still far from expert human-level, which suggests several area of improvements, including less reliance on object detection for grounding linguistic representations with visual sources, as well as finer-grained multimodal groundings.

Our work sheds light on future research in: (1) more generally applicable multimodal models, and (2) better transfer learning techniques in low resource domains such as scientific articles (Gururangan et al. 2020). We summarize our main contributions as follows:

- A multimodal dataset mapping compound figures and associated captions from biomedical research articles to the labels of experiment methodologies , to help spur the research on multimodal understanding for scientific articles.
- We conducted extensive experiments to benchmark and analyze various unimodal and multimodal models against the proposed dataset, suggesting several future directions for multimodal models in scientific domain.

The MELINDA Dataset

We introduce a new multimodal dataset, MELINDA, for biomedical experiment method classification. Each data instance is a unique tuple consisting of a figure, an associated sub-caption for the targeted sub-figure(s), and an experiment method label coming from the IntAct database. IntAct stores manually annotated labels for experiment method types, paired with their corresponding sub-figure identifiers and ids to the original paper featuring the figures[3], and structures them into an ontology. Each major category have different levels of granularity. This work mainly focuses on two major categories of experiments for identifying molecular interactions: *participant identification (Par)* and *interaction detection (Int)* methods[4], each has two levels of granularity, coarse and fine (choice of the granularity depends on downstream applications). Samples of data and their labels are as exemplified in Figure 2 (more are in the appendix).

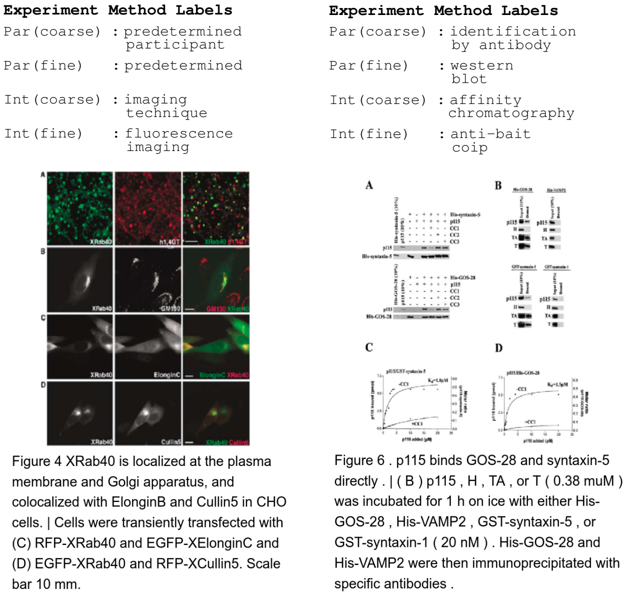

```
Experiment Method Labels
Par(coarse) : predetermined
              participant
Par(fine)   : predetermined
Int(coarse) : imaging
              technique
Int(fine)   : fluorescence
              imaging
```

Figure 4 XRab40 is localized at the plasma membrane and Golgi apparatus, and colocalized with ElonginB and Cullin5 in CHO cells. | Cells were transiently transfected with (C) RFP-XRab40 and EGFP-XElonginC and (D) EGFP-XRab40 and RFP-XCullin5. Scale bar 10 mm.

```
Experiment Method Labels
Par(coarse) : identification
              by antibody
Par(fine)   : western
              blot
Int(coarse) : affinity
              chromatography
Int(fine)   : anti-bait
              coip
```

Figure 6 . p115 binds GOS-28 and syntaxin-5 directly . | (B) p115 , H , TA , or T (0.38 muM) was incubated for 1 h on ice with either His-GOS-28 , His-VAMP2 , GST-syntaxin-5 , or GST-syntaxin-1 (20 nM) . His-GOS-28 and His-VAMP2 were then immunoprecipitated with specific antibodies .

Figure 2: Sample data: The basic structure of the data in MELINDA is composed of a figure, a sub-caption associated to one or multiple sub-figure(s), and a set of curated experiment method labels as shown on top of each figure. These labels represent the types of experiments conducted to generate the shown resulting sub-figures and captions. The above left sample concerns sub-figures (C) and (D), while the right sample concerns sub-figure (B), as indicated in their captions. Human experts tend to determine the labels leveraging features such as scientific terms concerning assays and methodologies in the captions, as well as indicative image features such as blots, graphs, and microscopic images.

Each record in IntAct consists of the aforementioned expert curated information to a specific article in the **Open Access PubMed Central**[5] (**OA-PMC**). According to the IntAct guideline, figure captions are sufficiently descriptive for justifying the underlying methods of the figures, and hence are properly extracted instead of including the body of text in the articles. The details of the dataset collection procedures and its statistics are described in the following sections.

Data Collection Pipeline

Our dataset is collected through three main procedures, as illustrated in Figure 3: (1) Obtain the experiment method labels and sub-figure identifiers from IntAct. (2) Localize the

[2] https://www.ebi.ac.uk/intact/

[3] IntAct only stores these ids as pointers, and our collection pipeline extracts the actual contents according to these pointers.

[4] Molecular interaction experiments require two types of assay: participant detection methods identify the molecules involved in the interaction and the interaction detection methods identify the types of interactions occurring between the two molecules.

[5] A publicly available subset of the PubMed collections: https://www.ncbi.nlm.nih.gov/pmc/tools/openftlist/

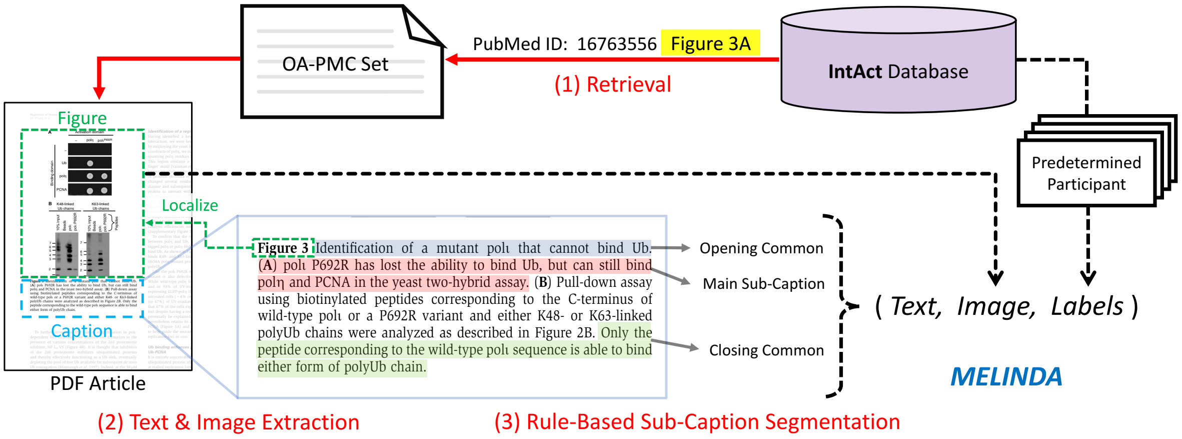

Figure 3 Identification of a mutant polι that cannot bind Ub. (**A**) polι P692R has lost the ability to bind Ub, but can still bind polη and PCNA in the yeast two-hybrid assay. (**B**) Pull-down assay using biotinylated peptides corresponding to the C-terminus of wild-type polι or a P692R variant and either K48- or K63-linked polyUb chains were analyzed as described in Figure 2B. Only the peptide corresponding to the wild-type polι sequence is able to bind either form of polyUb chain.

Figure 3: Data collection pipeline: Our collection pipeline is *distantly supervised* and fully automatable. It consists of three main steps: (1) Retrieve the PDF article in the OA-PMC set using the PubMed id from the IntAct database. (2) Extract the caption blocks using an in-house PDF interpreter, and localize the nearby corresponding figures. (3) Segment the caption blocks into sub-captions. Combining all three steps with the paired labels gives a single data record in our MELINDA dataset.

indicated figures and their captions in the pointed PDF articles. (3) Segment the captions into sub-captions so each can target a sub-figure of the figures obtained in step (2). As the overall procedure adopts a fully automated *distant supervision* approach, our dataset could be *seamlessly expanded as additional articles being added* to the OA-PMC set.

Ground Truth IntAct Label Extraction. By properly parsing and mapping the *PSI-MI2.5*[6] formatted IntAct records, each individually extracted instance can form a unique tuple of $(\textit{experiment-method-labels}, \textit{sub-figure-id})$, where the *sub-figure-id* is a concatenation of the PubMed id of an article and the sub-figure identifier.

Text and Image Extraction. The OA-PMC paper ids are then used to search and download the indicated PDF articles. The textual and image contents are extracted using an in-house PDF interpreter, which leverages spatial indexing over each page to support content extractions. We extract contiguous word blocks across the articles, and the figure captions are localized by detecting the keywords ‘Fig’ or ‘Figure’. The corresponding figures are cropped out by searching for large rectangular regions with low text densities nearby the captions. Note that although the classification task concerns sub-figures, **we do not further segment a figure into sub-figures** as we expect the models to be equipped with the capability of attending to the right sub-figures given the captions. Moreover, there are captions cross-referencing multiple sub-figures, and thus full figures should be preserved.

Sub-Caption Segmentation. Captions for compound figures are first tokenized into sentences followed by a text cleansing preprocessing, and then grouped into proper corresponding sub-captions through the following steps: (1) Descriptions before the first sentence containing sub-figure identifiers, *e.g.* ”(A)”, ”(A-C)”, are extracted as the *opening common* text. (2) The sentence containing a detected sub-figure identifier and all of its subsequent ones until the next sentence containing different identifier(s) is found, are extracted as the *main* sub-caption for that particular identifier. (3) Descriptions after the last sentence containing identifiers, are regarded as the *closing common* text, as researchers may put some summary texts at the end. Hence, a proper sub-caption is a concatenation of all of the above, which ensures no relevant contents of a sub-caption is overlooked. More details of our data collection pipeline can be found in the appendix and our released code repository[7].

Data Quality Assessment

Since our dataset is created by distant supervision from IntAct, for which if we perfectly pair the labels with corresponding figures and subcaptions, the *expert* human performances should remain ~100%. Therefore, the quality of the data instances rely on the quality of content extraction and pairing. In order to estimate the quality of the extracted contents, we randomly sample 100 instances for a manual inspection. With the corresponding original papers provided, we ask three non-domain-expert annotators to assess the quality mainly in terms of how good the image cropping is and how accurate the caption extractions are (the results were computed via majority vote). The inter-annotator agreement Fleiss’ Kappa for the following results are 0.804 for images and 0.676 for captions assessments.

Table 1a shows the inspection results of the extracted (and cropped) images on if they are missing any important regions, or containing any noises. Among the sampled images, 92% (*i.e.* 34+58) of the images are showing reasonably good quality, with 8% of them missing some details due to the cropping. The quality of the extracted (and segmented)

[6] An XML format: http://psidev.info/mif

[7] The data collection pipeline and our benchmark models can be found at https://github.com/PlusLabNLP/melinda.

Quality	Descriptions	%
☹	Imperfect crop of the figures, *i.e.* accidentally cropped out some parts	8
☺	Perfect crop of figures but with some small additional nuisances *e.g.* partial captions, other figures, etc.	34
	Perfect nuisance-free crop of figures with proper boundaries	58

(a) Image cropping quality assessments

Quality	Descriptions	%
☹	Extracted captions do not match the original captions in the PDF or the extracted figures (caption-figure mismatch)	4
☺	Extracted and segmented sub-captions match the original sub-captions in the PDF and caption-figure matched	10
	Sub-captions matched the original sub-captions in the PDF with *common* parts preserved and caption-figure matched	86

(b) Caption extraction & segmentation quality assessments

Table 1: Data quality assessments out of 100 random samples: For both (a) image cropping and (b) caption extraction and segmentation, the assessments show there are over 90% of samples regarded as good (☺), while there is a small proportion with certain noises in the extractions (☹).

sub-captions, as well as whether they match the associated sub-figure images, is summarized in Table 1b. Over 96% of the sampled data can be regarded as good, while 4% of them have issues such as partial texts missing. It is worth noting that even in this proportion of data which misses some details, the majority parts of the captions (and the figures) are still properly preserved.

Dataset Details

General Statistics. There are in total 5,371 data instances in our dataset, generated from 1,497 OA-PMC articles, with 2,833 uniquely extracted images, as summarized in table 2. The total unique label counts of each level in the original IntAct database as well as our collected dataset is summarized in Table 3. Figure 4a shows the histogram of caption word counts of the whole dataset, where the words are tokenized by applying simple NLTK word tokenizer on each caption, and the histogram of sentence counts in a caption is as shown in Figure 4b. The top-30 frequent words (stop words and punctuation excluded) of the whole dataset are visualized in Figure 5, with lemmatization applied.

Data Splits. We split the whole dataset into three subsets: train, validation, and test sets, with a ratio of 80% – 10% – 10%. In order to prevent models from exploiting certain patterns in the same article to make predictions, we assure that no data records extracted from the same paper is split into different subsets. Additionally, we ensure that the labels are distributed evenly in the three sets according to the coarse *participant* method, as illustrated in Figure 6.

Type	Counts			
Total Unique Articles	1,497			
Total Unique Images	2,833			
Total Data Instances	5,371			
Train / Val / Test	4,344 / 449 / 578			
Type-Token Ratio	29,384 / 501,091 = 0.059			
Type	**Mean**	**Std**	**Min**	**Max**
Tokens in a Caption	93.29	47.33	3	491
Sentences in a Caption	5.23	2.36	1	27
Tokens in a Sentence	17.83	12.27	1	256

Table 2: General statistics of MELINDA: We provide the detailed component counts of our dataset, including the sizes for each split (upper half), and the statistics of tokens and sentences from the captions (lower half).

Method Category	Hierarchy	# IntAct Labels	# Labels in Our Dataset
Participant	Coarse	7	7
	Fine	48	45
Interaction	Coarse	18	15
	Fine	122	85

Table 3: Unique IntAct label counts: For each of the main categories, *participant* and *interaction*, we list the number of unique labels in the original IntAct database and our collected dataset, for both the coarse and fine-grained labels.

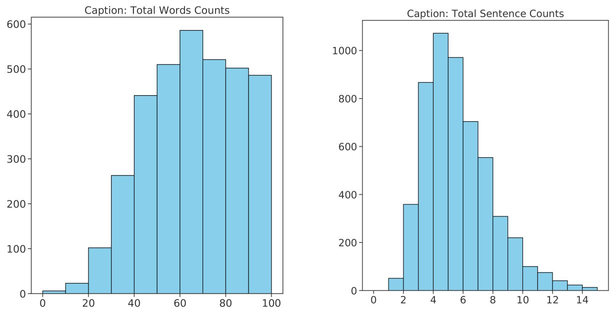

(a) Word Counts.

(b) Sentence Counts.

Figure 4: Word & sentence histograms: the histograms of *per caption* word and sentence counts. The charts can be examined jointly with Table 2 for better understandings.

Benchmark Models

We benchmark several state-of-the-art vision, language and multimodal models against our dataset, that differ primarily by the modalities they encode. Specifically, we consider unimodal models which take either an image (image-only) or a caption (caption-only) as input, and multimodal models that take both. All the output layers for classification are multilayer perceptrons (MLPs) followed by a softmax layer.

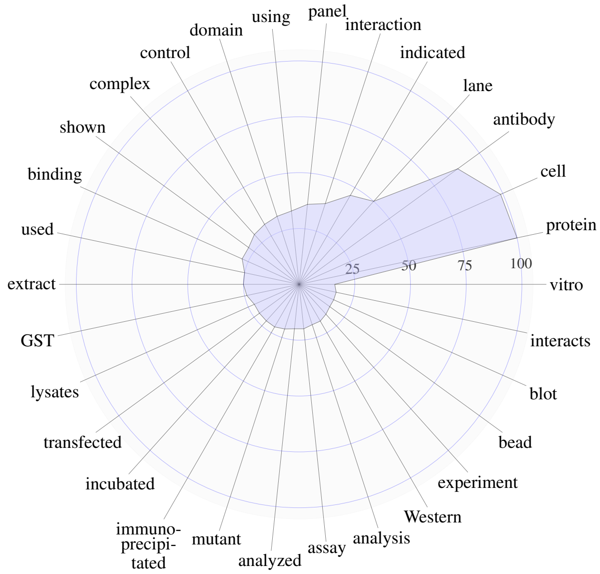

Figure 5: Top-30 frequent words: We normalize the word counts w.r.t the most frequent word (lemmatization applied), *protein*, which has 4280 appearances (*i.e*. denoted as 100%).

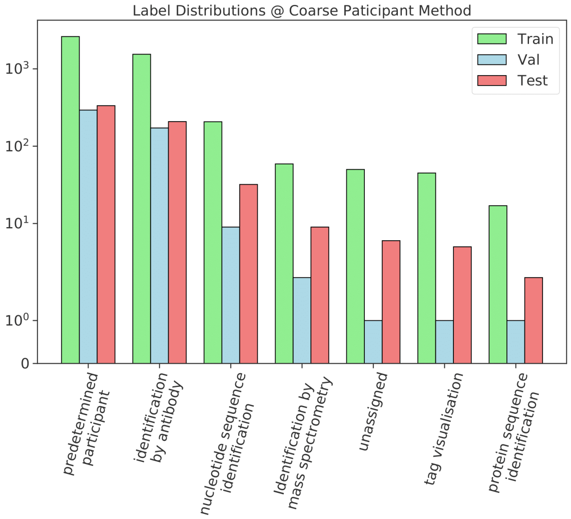

Figure 6: Label distributions: with respect to the *participant (coarse)* label type for each data split. We compute the number of data records of each unique ground truth labels. The y-axis is log scaled. The top two classes are: *predetermined participant*, and *identification by antibody*.

Unimodal Models

- **Image-Only**: We adopt a variant of convolutional neural networks, ResNet-101 (He et al. 2016), and initialize the networks with two sets of pretrained weights: (1) ImageNet classification task (Deng et al. 2009), and (2) backbone of Mask R-CNN on object detection task (He et al. 2017). We finetune the final three ResNet blocks (from a total of five), given the consistency of early level features across visual domains (more details in the appendix).
- **Caption-Only**: We mainly consider the two de-facto variants of language models: LSTM-based (Hochreiter and Schmidhuber 1997), and transformer-based (Vaswani et al. 2017) models. Our LSTM models take input word embeddings from Bio-GloVe (300-d) (Burns, Li, and Peng 2019). For transformer-based models, we consider two state-of-the-art pretrained masked language models (**MLM**): BERT (Devlin et al. 2019) trained on scientific corpora, dubbed SciBERT (Beltagy, Lo, and Cohan 2019), and RoBERTa (Liu et al. 2019b).

We experiment caption-only models with and without the **masked language finetuning on the caption sentences of our dataset**, by constructing a corpus where each sentence is a caption from the train and validation sets. We use RoBERTa-large and uncased version of SciBERT to initialize the language models' weights.

Multimodal Models

- **Naive Late Fusion (NLF)**: The images and captions are encoded by its best performing unimodal models – ResNet (ImageNet weights) and SciBERT respectively, which are then concatenated (late fusion) and fed into MLPs.
- **Stacked Attention Network (SAN)** (Yang et al. 2016): is a multi-step co-attention based framework that has demonstrated good performances on Visual Question Answering (VQA) benchmark (Antol et al. 2015). The image and caption encoders are same as in NLF.
- **ViL-BERT**: Vision-and-Language BERT (Lu et al. 2019), an extension of BERT model which learns a joint visual-and-linguistics representation through co-attentional transformer layers on top of unimodal visual and textual streams. The model has two major proxy pretraining objectives: (1) textual and visual masked learning, where the visual stream requires the model to predict missing masked-out regions of input images (**visual-MLM**), and (2) image-text alignment prediction, which extends BERT's next sentence prediction (**NSP**).
- **VL-BERT**: As the concurrent work to ViL-BERT, the visual-linguistics BERT model (Su et al. 2020) (VL-BERT) performs the multimodal co-attention in an early fusion manner with a single stream of transformer models. VL-BERT also adopts textual and visual masked learning pretraining objectives, while excluding the image-text multimodal alignment prediction.

The two multimodal BERT models are initialized with the SciBERT pretrained weights directly to their textual parts. For both ViL-BERT and VL-BERT, the visual-MLM leverages region of interests (ROIs) proposed by the object detection module, as well as the predicted class labels with high confidences. Due to significant domain shifts between the pretrained object detectors and our dataset, we experiment inclusion and exclusion of various of their proposed pretraining objectives (mainly concerning the visual masked prediction) when *finetuning on our dataset*.

Modalities	Models	Variants	Par$_{\text{coarse}}$	Int$_{\text{coarse}}$	Par$_{\text{fine}}$	Int$_{\text{fine}}$
—	Majority Baseline	—	55.88	63.67	48.96	23.18
Image-Only	ResNet-101	init. from ImageNet	63.84	70.24	50.87	28.50
		init. from MSCoCo	59.52	70.07	50.35	29.20
Caption-Only	LSTM w. BioGloVe	—	59.20	68.02	49.00	35.30
	RoBERTa	w/o MLM finetuning	74.60	86.00	60.00	64.70
		w. MLM finetuning	75.40	88.60	63.00	67.10
	SciBERT	w/o MLM finetuning	76.60	86.70	62.10	65.70
		w. MLM finetuning	77.70	87.00	64.90	67.10
Multi-Modal	NLF	w/o language part MLM finetuning	76.60	88.10	61.10	67.30
		w. language part MLM finetuning	73.70	87.90	62.80	70.20
	SAN	w/o language part MLM finetuning	72.30	88.60	61.90	70.40
		w. language part MLM finetuning	71.60	88.90	62.80	70.40
	ViL-BERT	w. MLM	78.20	90.64	66.26	72.15
		w. MLM & NSP	**78.60**	**90.83**	65.57	72.84
		w. MLM & NSP & visual-MLM	76.47	90.48	64.19	71.80
	VL-BERT	w. MLM	78.02	89.96	**66.49**	**74.65**
		w. MLM & visual-MLM	77.90	89.76	65.82	74.02

Table 4: Model accuracies on the test set: the two label categories are denoted as *Par*, and *Int* for *participant* and *interaction* method respectively. The label hierarchy is indicated as the subscript, *e.g.* Par$_{coarse}$ indicates coarse types of *participant* method. The best performances for each type of labels are bolded, and in all cases the two advanced multimodal models achieve the best performances. Particularly for the two multimodal models, the variants without the visual-MLM objectives are the best.

Experiments and Analysis

Our experiments aim to: (1) Benchmark the performances of the baseline models described in the previous section, and (2) compare and analyze how and what these models learn.

Quantitative Results. Table 4 summarizes the model performances on the test set, including the majority baseline that selects the most frequent classes in different label types. All the models, after training on the train set, outperform the majority baseline by large margins, which indicates the sizable training set is effective in transferring knowledge learned from these pretrained models. The image-only models, despite not having indicators of which sub-figure to look at, still surpass the majority baseline, which we hypothesize that the models still learn the salience in the images to make the correct predictions. Both transformer-based caption-only models benefit from the masked language finetuning on our dataset, we hypothesize that such finetuning objective can alleviate severe domain shifts between the original pretraining corpora and our MELINDA corpus. Among all the models, the two visual-linguistics multimodal models show the best performances on all types of labels, especially on the **fine-grained types** (*i.e.* *Par*$_{fine}$ and *Int*$_{fine}$). We believe that when granularity is finer, more subtle complementary multimodal understanding is required. The non-transformer-based multimodal models (NLF and SAN), however, are either on par or worse than the best caption-only models, SciBERT, suggesting that the attention mechanism in transformers may be a substantially better basis for grounding multimodal and complementary information.

The image-only models initialized with classification weights outperforms the one with detection weights, which may hint that the object detectors can be more prone to the *common objects* seen in their original training datasets. Such hypothesis is also shown in the performance comparisons within the visual-linguistics multimodal models, where they tend to perform better without the visual-MLM objective. However, within ViL-BERT, the multimodal alignment objective shown to be beneficial in most label types. In general, there are still huge gaps between model accuracies and expert human performances (∼100% accuracy), especially for the fine-grained types.

Visualizing What Models Learn. We utilize *Grad-CAM* (Selvaraju et al. 2017) for visualizing the model salience on the images and *SmoothGrad* (Smilkov et al. 2017) on the captions. Figure 7 shows a sampled side-by-side comparisons between unimodal models (left) and multimodal models (right) of label type ***Int***$_{coarse}$. It can be seen that the salience on the images clearly transition from being more dispersed to more detailed and finer-grained from unimodal to multimodal models. Likewise, multimodal models attend less on the common words such as *from*, *and*, *of*, and weight more on domain specific words. The image-only models, without the disambiguation from the captions, tend to focus more on spurious patterns as hinted in the first and second row. While the multimodal models exhibit diverged attentions in the images, it captures the keyword *fluorescence* that the unimodal language model fails to grasp. The third row of Figure 7 shows a failure case of multimodal models, where both unimodal models focused closer to the ideal regions in their inputs (note the sub-figure identifier ”*(a)*” in the caption), and hence make the correct predictions. We hypothesize that multimodal models may capture wrong information due to relatively stronger influences by the ROIs proposed by the inherited object detection module (refer to the overlaid yellow-colored ROIs).

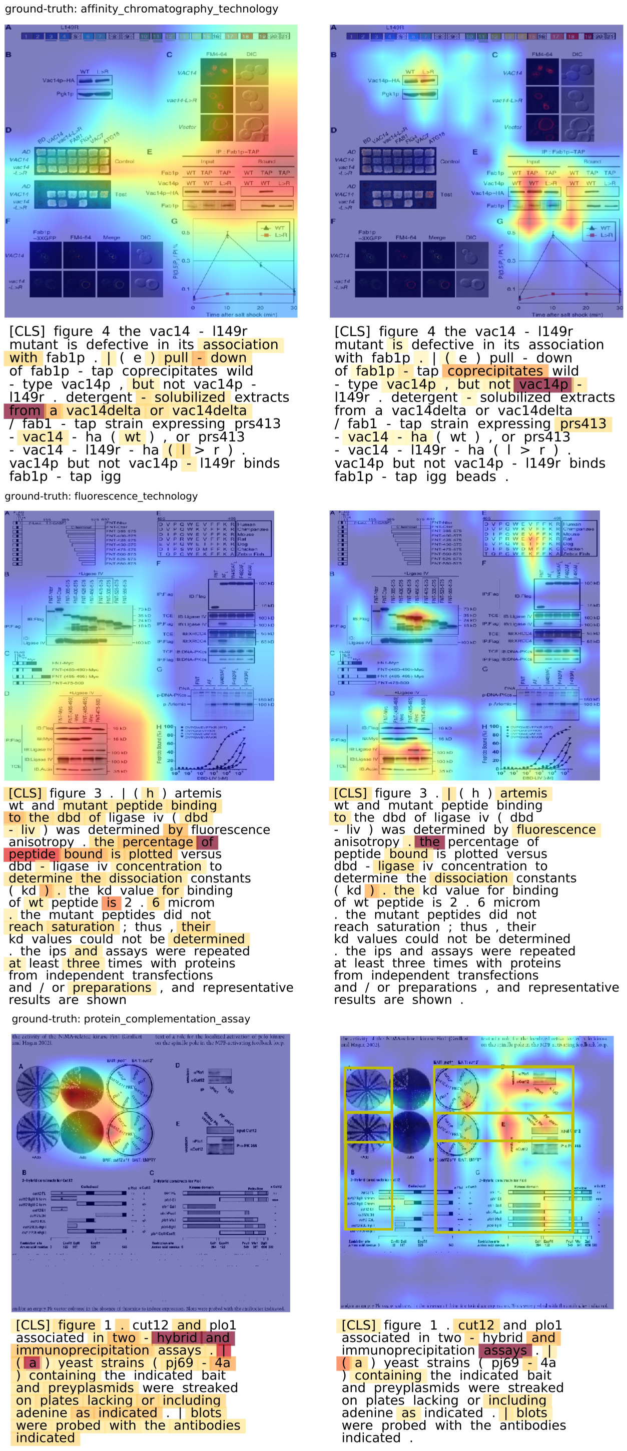

ground-truth: affinity_chromatography_technology

[CLS] figure 4 the vac14 - l149r mutant is defective in its association with fab1p . | (e) pull - down of fab1p - tap coprecipitates wild - type vac14p , but not vac14p - l149r . detergent - solubilized extracts from a vac14delta or vac14delta / fab1 - tap strain expressing prs413 - vac14 - ha (wt) , or prs413 - vac14 - l149r - ha (l > r) . vac14p but not vac14p - l149r binds fab1p - tap igg

[CLS] figure 4 the vac14 - l149r mutant is defective in its association with fab1p . | (e) pull - down of fab1p - tap coprecipitates wild - type vac14p , but not vac14p - l149r . detergent - solubilized extracts from a vac14delta or vac14delta / fab1 - tap strain expressing prs413 - vac14 - ha (wt) , or prs413 - vac14 - l149r - ha (l > r) . vac14p but not vac14p - l149r binds fab1p - tap igg beads .

ground-truth: fluorescence_technology

[CLS] figure 3 . | (h) artemis wt and mutant peptide binding to the dbd of ligase iv (dbd - liv) was determined by fluorescence anisotropy . the percentage of peptide bound is plotted versus dbd - ligase iv concentration to determine the dissociation constants (kd) . the kd value for binding of wt peptide is 2 . 6 microm . the mutant peptides did not reach saturation ; thus , their kd values could not be determined . the ips and assays were repeated at least three times with proteins from independent transfections and / or preparations , and representative results are shown

[CLS] figure 3 . | (h) artemis wt and mutant peptide binding to the dbd of ligase iv (dbd - liv) was determined by fluorescence anisotropy . the percentage of peptide bound is plotted versus dbd - ligase iv concentration to determine the dissociation constants (kd) . the kd value for binding of wt peptide is 2 . 6 microm . the mutant peptides did not reach saturation ; thus , their kd values could not be determined . the ips and assays were repeated at least three times with proteins from independent transfections and / or preparations , and representative results are shown .

ground-truth: protein_complementation_assay

[CLS] figure 1 . cut12 and plo1 associated in two - hybrid and immunoprecipitation assays . | (a) yeast strains (pj69 - 4a) containing the indicated bait and preyplasmids were streaked on plates lacking or including adenine as indicated . | blots were probed with the antibodies indicated

[CLS] figure 1 . cut12 and plo1 associated in two - hybrid and immunoprecipitation assays . | (a) yeast strains (pj69 - 4a) containing the indicated bait and preyplasmids were streaked on plates lacking or including adenine as indicated . | blots were probed with the antibodies indicated .

(a) Image-only & Text-only

(b) Multimodal

Figure 7: Saliency on $\text{Int}_{\text{coarse}}$ (highest-lowest attention → images – red-blue, and captions – dark red-light yellow: In each row: (a) *independent* unimodal models – ResNet-101 & SciBERT, (b) multimodal model – VL-BERT. From top to bottom the correctness of predictions between (a, b) are: (✓, ✓), (✗, ✓), and (✓, ✗). Top ROIs are shown on the failure case of multimodal model (third row), where they co-locate with the highest attended regions.

Related Works

Multimodal Datasets. There are numerous datasets for multimodal machine learning in existence, including visual storytelling (Huang et al. 2016), visual-linguistics reasoning (Johnson et al. 2017; Hasan et al. 2019; Wang et al. 2019; Liu et al. 2020), and multimodal question answering (QA) (Antol et al. 2015; Tapaswi et al. 2016; Kembhavi et al. 2016, 2017; Lei et al. 2018; Yagcioglu et al. 2018; Das et al. 2018; Zellers et al. 2019). As these works focus on more general domains, our work offers a dataset in the hope of motivating research in domains that often require expertise for labelling, such as biomedical.

Experiment Method Classification. The closest prior work (Burns, Li, and Peng 2019) has used the figure captions from OA-PMC set to perform similar experiment method classification task. In our MELINDA dataset, we put forth to extract the visual information in conjunctions with the caption texts, and collect a larger-scale dataset.

Automating Biocuration & Biomedical Tasks. Integrating computational approaches into the workflow of biocuration can be seen in many applications such as constructing genomics knowledge base (Baumgartner Jr et al. 2007), biomedical document classification (Cohen 2006; Shatkay, Chen, and Blostein 2006; Jiang et al. 2017; Simon et al. 2019), biomedical text mining (Dowell et al. 2009), and human-in-the-loop curation (Lee et al. 2018). Some prior works also adopt multimodal machine learning for general biomedical information extractions (Schlegl et al. 2015; Eickhoff et al. 2017; Zhang et al. 2017), as well as textual extraction (Burns, Dasigi, and Hovy 2017), medical image captioning (Shin et al. 2016), and automated diagnosis from medical images (Jing, Xie, and Xing 2018; Wang et al. 2018; Liu et al. 2019a).

Our work aims to further facilitate research in automating biocuration by providing a sizeable multimodal dataset, along with the data collection tool. We benchmark various unimodal and multimodal models with analysis on their strengths that suggest potential improvements.

Conclusions and Future Work

In this work, we introduce a new multimodal dataset, MELINDA, for biomedical experiment method classification. Our dataset comprises extracted image-caption pairs with the associated experiment method labels. As our data is collected in a fully automated *distant supervision* manner, the dataset is easily expandable.

We benchmark the proposed dataset against various baseline models, including state-of-the-art vision models, language models, and multimodal (visual-linguistics) models. The results show that despite multimodal models generally demonstrate superior performances, there are still huge rooms for improvements in the current visual-linguistics grounding paradigms, especially for domain specific data. Hence, we hope this work could motivate the future advancements in multimodal models, primarily on: (1) low resource domains and better transfer learning. (2) a less-supervised multimodal grounding method with less reliance on robust pretrained *object detectors*.

Acknowledgements

We thank the anonymous reviewers for their feedback, Yu Hou and Nuan Wen for their quality assessment annotations. This work is supported by a National Institutes of Health (NIH) R01 grant (LM012592). The views and conclusions of this paper are those of the authors and do not reflect the official policy or position of NIH.

References

Antol, S.; Agrawal, A.; Lu, J.; Mitchell, M.; Batra, D.; Lawrence Zitnick, C.; and Parikh, D. 2015. Vqa: Visual question answering. In *Proceedings of the IEEE Conference on Computer Vision and Pattern Recognition (CVPR)*, 2425–2433.

Baumgartner Jr, W. A.; Cohen, K. B.; Fox, L. M.; Acquaah-Mensah, G.; and Hunter, L. 2007. Manual curation is not sufficient for annotation of genomic databases. In *Bioinformatics*, volume 23, i41–i48. Oxford University Press.

Beltagy, I.; Lo, K.; and Cohan, A. 2019. SciBERT: Pretrained Language Model for Scientific Text. In *Empirical Methods in Natural Language Processing (EMNLP)*.

Ben Abacha, A.; Hasan, S. A.; Datla, V. V.; Liu, J.; Demner-Fushman, D.; and Müller, H. 2019. VQA-Med: Overview of the Medical Visual Question Answering Task at ImageCLEF 2019. In *CLEF2019 Working Notes*, CEUR Workshop Proceedings. Lugano, Switzerland: CEUR-WS.org <http://ceur-ws.org>.

Burns, G.; Shi, X.; Wu, Y.; Cao, H.; and Natarajan, P. 2018. Towards Evidence Extraction: Analysis of Scientific Figures from Studies of Molecular Interactions. In *ISWC (Best Workshop Papers)*, 95–102.

Burns, G. A.; Dasigi, P.; and Hovy, E. H. 2017. Extracting evidence fragments for distant supervision of molecular interactions. In *BioRxiv*, 192856. Cold Spring Harbor Laboratory.

Burns, G. A.; Li, X.; and Peng, N. 2019. Building deep learning models for evidence classification from the open access biomedical literature. In *Database*, volume 2019. Narnia.

Chen, Y.-C.; Li, L.; Yu, L.; Kholy, A. E.; Ahmed, F.; Gan, Z.; Cheng, Y.; and Liu, J. 2020. Uniter: Learning universal image-text representations. In *European Conference on Computer Vision (ECCV)*.

Cohen, A. M. 2006. An effective general purpose approach for automated biomedical document classification. In *AMIA annual symposium proceedings*, volume 2006, 161. American Medical Informatics Association.

Craven, M.; Kumlien, J.; et al. 1999. Constructing biological knowledge bases by extracting information from text sources. In *ISMB*, volume 1999, 77–86.

Das, A.; Datta, S.; Gkioxari, G.; Lee, S.; Parikh, D.; and Batra, D. 2018. Embodied question answering. In *Proceedings of the IEEE Conference on Computer Vision and Pattern Recognition (CVPR)*, 2054–2063.

Demner-Fushman, D.; Antani, S.; Simpson, M.; and Thoma, G. R. 2012. Design and development of a multimodal biomedical information retrieval system. In *Journal of Computing Science and Engineering*, volume 6, 168–177. Korean Institute of Information Scientists and Engineers.

Deng, J.; Dong, W.; Socher, R.; Li, L.-J.; Li, K.; and Fei-Fei, L. 2009. Imagenet: A large-scale hierarchical image database. In *Proceedings of the IEEE Conference on Computer Vision and Pattern Recognition (CVPR)*, 248–255.

Devlin, J.; Chang, M.-W.; Lee, K.; and Toutanova, K. 2019. BERT: Pre-training of Deep Bidirectional Transformers for Language Understanding. In *North American Chapter of the Association for Computational Linguistics (NAACL-HLT)*, 4171–4186.

Dowell, K. G.; McAndrews-Hill, M. S.; Hill, D. P.; Drabkin, H. J.; and Blake, J. A. 2009. Integrating text mining into the MGI biocuration workflow. In *Database*, volume 2009. Narnia.

Eickhoff, C.; Schwall, I.; García Seco de Herrera, A.; and Müller, H. 2017. Overview of ImageCLEFcaption 2017 - the Image Caption Prediction and Concept Extraction Tasks to Understand Biomedical Images. In *CLEF (Working Notes)*, CEUR Workshop Proceedings. Dublin, Ireland: CEUR-WS.org <http://ceur-ws.org>.

Gururangan, S.; Marasović, A.; Swayamdipta, S.; Lo, K.; Beltagy, I.; Downey, D.; and Smith, N. A. 2020. Don't Stop Pretraining: Adapt Language Models to Domains and Tasks. *arXiv preprint arXiv:2004.10964* .

Hasan, M. K.; Rahman, W.; Zadeh, A.; Zhong, J.; Tanveer, M. I.; Morency, L.-P.; et al. 2019. UR-FUNNY: A multimodal language dataset for understanding humor. In *Empirical Methods in Natural Language Processing (EMNLP)*.

He, K.; Gkioxari, G.; Dollár, P.; and Girshick, R. 2017. Mask r-cnn. In *International Conference on Computer Vision (ICCV)*, 2961–2969.

He, K.; Zhang, X.; Ren, S.; and Sun, J. 2016. Deep residual learning for image recognition. In *Proceedings of the IEEE Conference on Computer Vision and Pattern Recognition (CVPR)*, 770–778.

He, X.; Zhang, Y.; Mou, L.; Xing, E.; and Xie, P. 2020. PathVQA: 30000+ Questions for Medical Visual Question Answering. *arXiv preprint arXiv:2003.10286* .

Hochreiter, S.; and Schmidhuber, J. 1997. Long short-term memory. In *Neural computation*, volume 9, 1735–1780. MIT Press.

Huang, T.-H.; Ferraro, F.; Mostafazadeh, N.; Misra, I.; Agrawal, A.; Devlin, J.; Girshick, R.; He, X.; Kohli, P.; Batra, D.; et al. 2016. Visual storytelling. In *North American Chapter of the Association for Computational Linguistics (NAACL-HLT)*, 1233–1239.

ISB. 2018. Biocuration: Distilling data into knowledge. In *PLOS Biology*, volume 16, 1–8. Public Library of Science. doi:10.1371/journal.pbio.2002846. URL https://doi.org/10.1371/journal.pbio.2002846.

Jiang, X.; Ringwald, M.; Blake, J.; and Shatkay, H. 2017. Effective biomedical document classification for identifying publications relevant to the mouse Gene Expression Database (GXD). In *Database*, volume 2017. Narnia.

Jing, B.; Xie, P.; and Xing, E. 2018. On the Automatic Generation of Medical Imaging Reports. In *Association for Computational Linguistics (ACL)*, 2577–2586. Melbourne, Australia: Association for Computational Linguistics. doi:10.18653/v1/P18-1240.

Johnson, J.; Hariharan, B.; van der Maaten, L.; Fei-Fei, L.; Lawrence Zitnick, C.; and Girshick, R. 2017. Clevr: A diagnostic dataset for compositional language and elementary visual reasoning. In *Proceedings of the IEEE Conference on Computer Vision and Pattern Recognition (CVPR)*, 2901–2910.

Kembhavi, A.; Salvato, M.; Kolve, E.; Seo, M.; Hajishirzi, H.; and Farhadi, A. 2016. A diagram is worth a dozen images. In *European Conference on Computer Vision (ECCV)*, 235–251. Springer.

Kembhavi, A.; Seo, M.; Schwenk, D.; Choi, J.; Farhadi, A.; and Hajishirzi, H. 2017. Are you smarter than a sixth grader? textbook question answering for multimodal machine comprehension. In *Proceedings of the IEEE Conference on Computer Vision and Pattern Recognition (CVPR)*, 4999–5007.

Lee, K.; Famiglietti, M. L.; McMahon, A.; Wei, C.-H.; MacArthur, J. A. L.; Poux, S.; Breuza, L.; Bridge, A.; Cunningham, F.; Xenarios, I.; et al. 2018. Scaling up data curation using deep learning: An application to literature triage in genomic variation resources. In *PLoS computational biology*, volume 14, e1006390. Public Library of Science.

Lei, J.; Yu, L.; Bansal, M.; and Berg, T. L. 2018. Tvqa: Localized, compositional video question answering. In *Empirical Methods in Natural Language Processing (EMNLP)*.

Li, L. H.; Yatskar, M.; Yin, D.; Hsieh, C.-J.; and Chang, K.-W. 2019. Visualbert: A simple and performant baseline for vision and language. *arXiv preprint arXiv:1908.03557* .

Liu, J.; Chen, W.; Cheng, Y.; Gan, Z.; Yu, L.; Yang, Y.; and Liu, J. 2020. VIOLIN: A Large-Scale Dataset for Video-and-Language Inference. In *Proceedings of the IEEE Conference on Computer Vision and Pattern Recognition (CVPR)*.

Liu, S.; Ou, X.; Che, J.; Zhou, X.; and Ding, H. 2019a. An Xception-GRU Model for Visual Question Answering in the Medical Domain. *CLEF (Working Notes)* .

Liu, Y.; Ott, M.; Goyal, N.; Du, J.; Joshi, M.; Chen, D.; Levy, O.; Lewis, M.; Zettlemoyer, L.; and Stoyanov, V. 2019b. Roberta: A robustly optimized bert pretraining approach. *arXiv preprint arXiv:1907.11692* .

Lu, J.; Batra, D.; Parikh, D.; and Lee, S. 2019. Vilbert: Pretraining task-agnostic visiolinguistic representations for vision-and-language tasks. In *Advances in Neural Information Processing Systems (NeurIPS)*, 13–23.

Mintz, M.; Bills, S.; Snow, R.; and Jurafsky, D. 2009. Distant supervision for relation extraction without labeled data. In *Proceedings of the Joint Conference of the 47th Annual Meeting of the ACL and the 4th International Joint Conference on Natural Language Processing of the AFNLP*, 1003–1011.

Mohan, S.; Fiorini, N.; Kim, S.; and Lu, Z. 2018. A fast deep learning model for textual relevance in biomedical information retrieval. In *Proceedings of the 2018 World Wide Web Conference*, 77–86.

Nguyen, B. D.; Do, T.-T.; Nguyen, B. X.; Do, T.; Tjiputra, E.; and Tran, Q. D. 2019. Overcoming Data Limitation in Medical Visual Question Answering. In *International Conference on Medical Image Computing and Computer-Assisted Intervention (MICCAI)*. Springer.

Orchard, S.; Ammari, M.; Aranda, B.; Breuza, L.; Briganti, L.; Broackes-Carter, F.; Campbell, N. H.; Chavali, G.; Chen, C.; Del-Toro, N.; et al. 2013. The MIntAct project—IntAct as a common curation platform for 11 molecular interaction databases. *Nucleic Acids Research (NAR)* 42(D1): D358–D363.

Schlegl, T.; Waldstein, S. M.; Vogl, W.-D.; Schmidt-Erfurth, U.; and Langs, G. 2015. Predicting semantic descriptions from medical images with convolutional neural networks. In *International Conference on Information Processing in Medical Imaging (IPMI)*, 437–448. Springer.

Selvaraju, R. R.; Cogswell, M.; Das, A.; Vedantam, R.; Parikh, D.; and Batra, D. 2017. Grad-cam: Visual explanations from deep networks via gradient-based localization. In *International Conference on Computer Vision (ICCV)*, 618–626.

Shatkay, H.; Chen, N.; and Blostein, D. 2006. Integrating image data into biomedical text categorization. In *Bioinformatics*, volume 22, e446–e453. Oxford University Press.

Shin, H.-C.; Roberts, K.; Lu, L.; Demner-Fushman, D.; Yao, J.; and Summers, R. M. 2016. Learning to read chest x-rays: Recurrent neural cascade model for automated image annotation. In *Proceedings of the IEEE Conference on Computer Vision and Pattern Recognition (CVPR)*, 2497–2506.

Simon, C.; Davidsen, K.; Hansen, C.; Seymour, E.; Barnkob, M. B.; and Olsen, L. R. 2019. BioReader: a text mining tool for performing classification of biomedical literature. In *BMC bioinformatics*, volume 19, 57. Springer.

Smilkov, D.; Thorat, N.; Kim, B.; Viégas, F.; and Wattenberg, M. 2017. Smoothgrad: removing noise by adding noise. In *International Conference on Machine Learning (ICML)*. Workshop on Visualization for Deep Learning.

Su, W.; Zhu, X.; Cao, Y.; Li, B.; Lu, L.; Wei, F.; and Dai, J. 2020. Vl-bert: Pre-training of generic visual-linguistic representations. In *International Conference on Learning Representations (ICLR)*.

Tapaswi, M.; Zhu, Y.; Stiefelhagen, R.; Torralba, A.; Urtasun, R.; and Fidler, S. 2016. Movieqa: Understanding stories in movies through question-answering. In *Proceedings of the IEEE Conference on Computer Vision and Pattern Recognition (CVPR)*, 4631–4640.

Vaswani, A.; Shazeer, N.; Parmar, N.; Uszkoreit, J.; Jones, L.; Gomez, A. N.; Kaiser, Ł.; and Polosukhin, I. 2017. Attention is all you need. In *Advances in Neural Information Processing Systems (NeurIPS)*, 5998–6008.

Wang, W.; Wang, Y.; Chen, S.; and Jin, Q. 2019. YouMakeup: A Large-Scale Domain-Specific Multimodal Dataset for Fine-Grained Semantic Comprehension. In *Proceedings of the 2019 Conference on Empirical Methods in Natural Language Processing and the 9th International Joint Conference on Natural Language Processing (EMNLP-IJCNLP)*, 5136–5146.

Wang, X.; Peng, Y.; Lu, L.; Lu, Z.; and Summers, R. M. 2018. Tienet: Text-image embedding network for common thorax disease classification and reporting in chest x-rays. In *Proceedings of the IEEE Conference on Computer Vision and Pattern Recognition (CVPR)*, 9049–9058.

Yagcioglu, S.; Erdem, A.; Erdem, E.; and Ikizler-Cinbis, N. 2018. Recipeqa: A challenge dataset for multimodal comprehension of cooking recipes. In *Empirical Methods in Natural Language Processing (EMNLP)*.

Yang, Z.; He, X.; Gao, J.; Deng, L.; and Smola, A. 2016. Stacked attention networks for image question answering. In *Proceedings of the IEEE Conference on Computer Vision and Pattern Recognition (CVPR)*, 21–29.

Zellers, R.; Bisk, Y.; Farhadi, A.; and Choi, Y. 2019. From recognition to cognition: Visual commonsense reasoning. In *Proceedings of the IEEE Conference on Computer Vision and Pattern Recognition (CVPR)*, 6720–6731.

Zhang, Z.; Chen, P.; Sapkota, M.; and Yang, L. 2017. Tandemnet: Distilling knowledge from medical images using diagnostic reports as optional semantic references. In *International Conference on Medical Image Computing and Computer-Assisted Intervention (MICCAI)*, 320–328. Springer.